Int. J. Electrochem. Sci., 14 **(2019)** 7348 – 7362, doi: 10.20964/2019.08.30

International Journal of
ELECTROCHEMICAL
SCIENCE
www.electrochemsci.org

Synergistic Effect of Phytic Acid and Benzyltrimethyl Ammonium Bromide on Corrosion Inhibition of Carbon Steel in 0.5 M HCl

Weipeng Zhang[1], *Zhe Zhang*[1], *Wenwu Li*[1], *Xiaodong Huang*[1], *Le Ruan*[1,*], *Ling Wu*[2]

[1] Guangxi Key Laboratory of Electrochemical and Magneto-chemical Functional Materials, College of Chemistry and Bioengineering, Guilin University of Technology, Guilin 541004, China.
[2] School of Chemistry and Chemical Engineering, Shandong University, Jinan 250100, PR China.
[*]E-mail: ruanle@glut.edu.cn

Received: 1 April 2019 / *Accepted:* 21 May 2019 / *Published:* 30 June 2019

The synergistic corrosion inhibition effect of phytic acid (PA) and benzyltrimethyl ammonium bromide (BAB) on 1045 carbon steel (CS) in 0.5 M HCl is reported. Electrochemical measurements showed that PA and BAB can reduce the corrosion rate of 1045 CS in HCl solution and act as excellent corrosion inhibitors. The best inhibition efficiency η_i of the combination inhibitor of PA with BAB is 90.6%. SEM images of the corroded steel surfaces suggest that the PA and BAB are simultaneously adsorbed on the CS surface to inhibit the corrosion of iron. The synergistic inhibition mechanism is investigated by dynamic simulations and quantum chemistry.

Keywords: Phytic acid; corrosion inhibition; HCl solution; dynamic simulations.

1. INTRODUCTION

Carbon steel as a common material is used extensively in many fields and plays an important role in industry, energy and so on that cannot be replaced[1, 2]. However, as a type of metal, it cannot avoid exposure to the air or direct contact with a liquid medium causing corrosion via oxidation and reduction, electrochemical reactions or dissolution. All of these factors result in large losses, substantial waste and can even cause very serious factory accidents. In recent years, the methods used to solve metal corrosion have mainly depended on traditional methods, e.g., covering the surface of the base metal with a coating or molecular form of the film. These compounds isolate the base metal from the corrosive medium to achieve corrosion protection.

.

The use of corrosion inhibitors is a traditional method of corrosion protection. It consists of one or more kinds of molecules. The inhibitor dose is trace with an appropriate concentration in the corrosive medium to achieve efficient corrosion protection. The inhibitor molecule of the film forms a layer or multi-layers to isolate the corrosive medium from the base metal to reduce the corrosion rate to zero[3, 4]. However, the addition of inhibitor to corrosive media cannot change the nature of the metal material. This is one of the advantages of an inhibitor. After long-term global exploration and research, researchers have found that molecules containing O, N, P and S atoms, which contain lone pair electrons that can be provided to the empty d-orbital of iron atoms to form a coordinate bond, are efficient corrosion inhibitors. The relative molecular mass of PA is 660.4, and the molecular formula is $C_6H_{18}O_{24}P_6$ with six phosphate groups. Therefore, PA is easily soluble in water with strong acidity. Figure 1 shows the structure of PA[5-7]. The unique cyclic structure and phosphate group are the key structural features that determine the inhibitory action. PA is extracted from innocuous and nonpoisonous plants and has abundant raw material sources and low cost[8-12]. In addition, many researchers have studied PA as a synergistic inhibitor to protect metal. Yanhua Lei, et al.[9] researched the properties of polypyrrole to form a film on copper from a PA solution in a NaCl solution for corrosion protection. However, the corrosion of carbon steel occurs in acidic corrosive media. The application of phytic acid to carbon steel protection via synergistic inhibitors is scarce in reports and documents. BAB is a highly efficient corrosion inhibitor. The BAB molecular formula is $C_{10}H_{16}N{\cdot}Br$. Figure 1 shows the structure of BAB. It is obvious that BAB contains one nitrogen atom, and its structure is similar to that of the highly effective inhibitor hexadecyl trimethyl ammonium bromide (CTAB)[13]. It has been reported that BAB has been applied to inhibit the corrosion of oil pipelines[14]. Therefore, we selected BAB as a synergistic inhibitor with PA. Therefore, this study investigated the corrosion inhibition of mild carbon steel in a 0.5 M HCl solution by the synergism of PA and BAB.

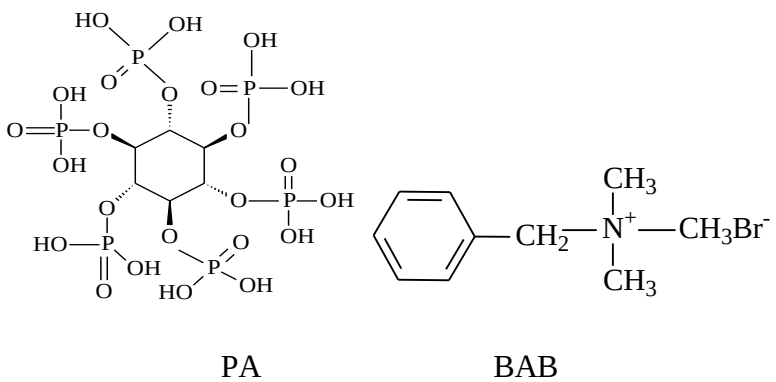

Figure 1. The structure of PA and BAB.

2. EXPERIMENTAL

2.1. Preparation of Electrodes

The working electrode (WE) was made of a 1045 carbon steel (CS) rod 2.5 cm in length with a cross-sectional area of 0.5024 cm^2. The chemical composition of the CS (wt.%) was C 0.45%, Si

0.17%, Mn 0.5%, S 0.035%, P 0.035%, Cr 0.25%, Cu 0.25%, Ni 0.30%, and Fe 98%. The carbon steel electrode was coasted in an epoxy resin and then electrical contacted with a copper wire. Before each experiment, the exposed surface was mechanically abraded with 800#, 1200# and 1400# emery papers until its surface was smooth and subsequently degreased and cleaned with ethanol using an ultrasonic cleaner. Then, the cleaned electrode was immersed in ethanol.[15].

2.2. Creation of synergistic inhibitor solutions

PA (70% in H_2O, Shanghai Macklin Biochemical Co., Ltd) was dissolved in 0.5 M HCl solution, which was prepared from analytical-grade HCl (12 M) and ultra-pure water at 25℃. Then BAB (≥98%, Aladdin Industrial Corporation) was dissolved in the PA solution with mechanical stirring. The molar ratio of the PA to BAB was 1:1, 1:2 and 1:3.

2.3. Electrochemical measurements

All electrochemical experiments were carried out in a traditional three-electrode system in a glass cell with two sheets of platinum foil (1.0 cm × 1.8 cm) as the counter electrodes and a saturated calomel electrode (SCE) as the reference electrode. Experiments were performed in 0.5 M HCl prepared from reagent-grade chemicals and ultra pure water. Electrochemical impedance spectroscopy (EIS) measurements were performed using an IM6 electrochemical workstation (ZAHNER, Germany). All the electrochemical measurements were performed after the WE was immersed in the test solution for 1 h, and the open circuit potential (E_{ocp}) remained stable. EIS was performed under the corrosion potential with a sinusoidal potential perturbation of 5 mV in amplitude, and the frequency was from 100 kHz to 0.1 Hz. The data from the EIS were fitted using the ZView2 software. The polarization curves were measured by dynamically scanning the potential at 2 $mV \cdot s^{-1}$ from Eocp -200 mV to Eocp +200 mV. The data for the polarization curves were fitted using the built-in IM6 software by the Tafel extrapolation method. All of the experiments were conducted at 25 ± 1 °C[15].

2.4. SEM Analysis

The corrosion surfaces were characterized by SEM (GSM-6380LV models of scanning electron microscopy, JEOL) using steel specimens (3 mm × 3 mm × 1 mm) corroded in synergistic inhibitor solutions prepared from 0.5 M HCl and inhibitor at 25℃ for 1 h.

2.5. Quantum chemical calculations and dynamic simulations

Gaussian 03 software[16] was used to perform the quantum chemical calculations using the B3LYP model of density functional theory (DFT) combined with the 6-311G (d, p) basis sets. Quantum chemical calculations were used to calculate the energy and optimize the geometric construction of the molecules. The function of B3LYP with 6-311G (d, p) can meet the needs

exactly[17-19]. The lowest unoccupied molecular orbital (E_{LUMO}), the highest occupied molecular orbital (E_{HOMO}), the value of the energy gap ($\Delta E = E_{LUMO} - E_{HOMO}$) and the dipole moment (μ) were calculated to evaluate the effect on the inhibition abilities.

Table 1. The details setup of molecular dynamics simulation.

Basic setup	Method	Conergence Level	Maximum iteration	
	smart minimizer	ultra-fine	20000	
Minimizer setup	Forcefield	Non-bond	Summation method	Cutoff distance
	compass	vdW	Atom based	9.5 Å
Dynamic simulation setup	Ensemble	Thermostat	Simulation temperature	Energy deviation
	NVT	Andersen	298.0 K	5000.0 kcal/mol
	Dynamic time	Time step	Frame output	
	2000.0 ps	1 fs	Every 1000 steps	

Molecular dynamic simulations were used to calculate the adsorption configuration of the inhibitor molecules on the iron surface, the water molecules and the Cl^- ion diffusion in the solution system by the Discover module of Materials Studio 6.0 software from AccelrysInc[20]. The system was at the temperature of 298 K. The dynamic simulations contained two parts: the solution layer and the iron base as the surface of the adsorbed molecules. The iron base is a box (24.8238 Å × 24.8238 Å × 18.2417 Å) with the periodic iron atom confined in the boundary conditions and the degree of zero vacuum. The Fe (1 1 0) crystal face was used as the base metal because the Fe (1 1 0) surface is a densely packed surface and therefore very stable[17, 21, 22]. From the Fe (1 1 0) surface, 10 layers of iron atoms were cleaved, and the energy of the box was optimized to a minimum. Part of the solution layer was a box (24.8238 Å × 24.8238 Å × 20.7286 Å) containing 400 H_2O, 5 H_3O^+, 5 Cl^- and 1 inhibitor molecule with the zero vacuum degree of the limited layer. Then, the energy of the solution layer was optimized to a minimum. The two parts and 100 H_2O of the limited layer create the dynamic simulation system. Before optimizing the entire system, the six-layer iron atoms must be frozen from the bottom and the H_2O-limited layer. Then, optimizing the entire system minimized the total energy of the system. Finally, the entire system reached a stable equilibrium state where the temperature and the energy of the system were stable. The details for the setup of the molecular dynamic simulation are listed in Table 1.

3. RESULTS AND DISCUSSION

3.1. Potentiodynamic polarization measurements

The potentiodynamic polarization curves with or without PA and BAB-modified CS in 0.5 M HCl are shown in Figure 2. The results showed that PA and BAB and their synergistic effect reduce

both the anodic dissolution of CS and the hydrogen evolution reaction. This result is attributed to the adsorption of PA and BAB and their synergistic molecules on the active sites of the CS surface.

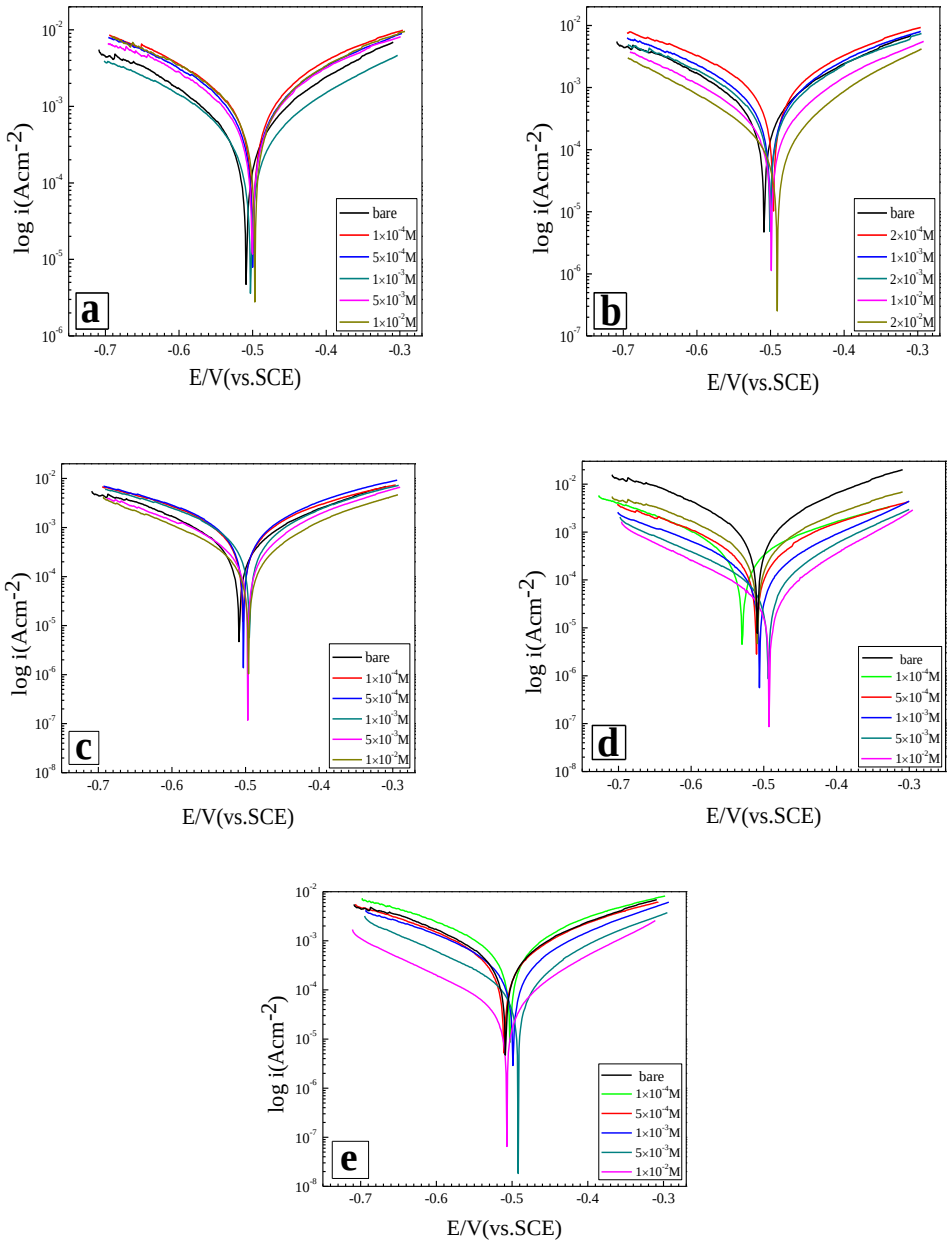

Figure 2. Carbon steel working electrode in the presence of different molar ratio or absence of corrosion inhibitor hydrochloric acid solution measured by the polarization curve, (a) is PA, (b) is BAB, (c) is PA : BAB = 1 : 1, (d) is PA : BAB = 1 : 2, (e) is PA : BAB = 1 : 3, the solid line is the impedance fitting curve.

The corrosion potential, corrosion current density, anodic Tafel slope and cathodic Tafel slope deduced from the polarization curves are given in Table 2. From Figure 2, it is clear that there is a small shift in the corrosion potential towards the anodic region. The anodic process is controlled by activation dissolution and no apparent passivation can be observed in the curves[23]. When the change

in the E_{corr} value is greater than 85 mV, an inhibitor can be classified as anodic or cathodic type[24-29]. The maximal shift value of E_{corr} is 10.9 mV (vs.SCE, Table 2) for the PA corrosion inhibitor with an assembling time of 1 h; the maximal shift value of E_{corr} is 18 mV for the BAB corrosion inhibitor with an assembling time of 1 h; and the maximal shift value of E_{corr} is 18.4 mV for both PA and BAB with an assembling time of 1 h. The small change in β_a and β_c (Tafel slopes) and E_{corr} means that all these inhibitors behave as a mixed type. The approximately parallel Tafel lines indicate that there is no change in the mechanism of CS corrosion[7, 30].

The inhibition efficiencies calculated from the values of the corrosion current density with and without inhibitor are shown in Table 1, according to Eq. (1):

$$\eta_i(\%) = \left(1 - \frac{i_{corr}}{i_{corr}^0}\right) \times 100\% \quad (1)$$

where i_{corr} and i_{corr}^0 are the corrosion current density values with and without the inhibitor, respectively, determined by extrapolation of the anodic and cathodic Tafel lines to the corrosion potentials. From Table 2, it can be observed that the inhibition efficiencies increase and then decrease for PA, and the maximal inhibition efficiency is 8.6% when the concentration is 1×10^{-3} M. When the concentration is above or below that value, the inhibition efficiency will decrease, even promoting corrosion. This result is because PA is a strong acid and has a strong chelating capacity. When the concentration of PA is lower, PA has a strong chelating ability and can combine with the iron ions of the carbon steel surface. PA will protect the carbon steel by providing lone pair electrons to iron atoms, forming a coordination bond. Then, a layer of corrosion-resistant film forms to protect the carbon steel against corrosion by HCl. Meanwhile, PA ionizes the hydrogen ions in water. As a strong acid, at a higher concentration, PA reduces the pH value to promote corrosion of the carbon steel substrate. Therefore, as the concentration of PA increases, the corrosion inhibition is stronger than the efficiency of corrosion promotion, and the protection efficiency reaches a maximum of 23.95% (Table 3) at a concentration of 1×10^{-3} M. When the concentration of PA is over 1×10^{-3} M, PA promotes corrosion[7, 31]. When the concentration is less than 2×10^{-3} M, BAB promotes corrosion, and the inhibition efficiency increases with increasing concentration. The reason may be that BAB will hydrolyse benzyl trimethyl ammonium cations and bromide ions in water. The benzyl trimethylammonium cations adsorbed on the carbon steel surface lead to a working electrode with a positive charge. This charge will attract Cl^- to the carbon steel surface to cause pitting. However, with the benzyl trimethylammonium cations covering the entire carbon steel surface, pitting will be inhibited, decreasing the rate of corrosion and the corrosion current. The synergy of PA and BAB with the optimal molar ratio for the inhibition efficiency is 1:2. This is because PA has a special ring structure that leaves some interspace between the PA molecules. However, BAB can fill up the interspaces in PA adsorbed on the carbon steel surface to further protect carbon steel from corrosion. When the molar ratio is 1:1, BAB cannot fill up the interspaces, and when the molar ratio is 1:3, competitive adsorption between molecules occurs. The values of β_a and, β_c exhibit no obvious changes, which suggests that the inhibition effect comes from the reduction in the reaction area on the corroded metal surface[32].

Table 2. Carbon steel working electrode in the presence or absence of corrosion inhibitor hydrochloric acid solution measured by the potential of the polarization curve parameters.

Assembly molecules	Concentration (mol.L^{-1})	Molar ratio	E (V vs.SCE)	$-\beta$c (V dec^{-1})	βa (V dec-1)	i_{corr} (μAcm^{-2})	η_i (%)
Bare	0	--	-0.5094	0.163	0.153	465	--
PA	1×10^{-4}	--	-0.5010	0.184	0.170	1269	-172.9
	5×10^{-4}	--	-0.4997	0.175	0.168	1024	-120.2
	1×10^{-3}	--	-0.5036	0.162	0.163	425	8.6
	5×10^{-3}	--	-0.5008	0.180	0.167	945	-103.2
	1×10^{-2}	--	-0.4985	0.185	0.171	1121	-141.1
BAB	2×10^{-4}	--	-0.4974	0.180	0.164	1056	-127.1
	1×10^{-3}	--	-0.5003	0.169	0.149	661	-42.2
	2×10^{-3}	--	-0.5014	0.158	0.140	529	-13.8
	1×10^{-2}	--	-0.4997	0.152	0.129	280	39.8
	2×10^{-2}	--	-0.4914	0.147	0.117	155	66.7
PA/BAB	1×10^{-4}	1:1	-0.5036	0.175	0.175	930	-100.0
	5×10^{-4}	1:1	-0.5036	0.178	0.167	972	-109.0
	1×10^{-3}	1:1	-0.4953	0.164	0.161	691	-48.6
	5×10^{-3}	1:1	-0.4975	0.176	0.139	406	12.7
	1×10^{-2}	1:1	-0.4972	0.148	0.128	229	50.8
PA/BAB	1×10^{-4}	1:2	-0.5278	0.145	0.183	339	27.1
	5×10^{-4}	1:2	-0.5092	0.168	0.160	325	30.1
	1×10^{-3}	1:2	-0.5052	0.155	0.138	157	66.2
	5×10^{-3}	1:2	-0.4955	0.154	0.113	81.4	82.5
	1×10^{-2}	1:2	-0.4923	0.139	0.099	43.5	90.6
PA/BAB	1×10^{-4}	1:3	-0.5034	0.165	0.151	633	-36.1
	5×10^{-4}	1:3	-0.5117	0.154	0.144	398	14.4
	1×10^{-3}	1:3	-0.4970	0.149	0.132	277	40.4
	5×10^{-3}	1:3	-0.4926	0.140	0.101	104	77.6
	1×10^{-2}	1:3	-0.5090	0.139	0.099	44.2	90.5

3.2. Electrochemical impedance spectroscopy measurements

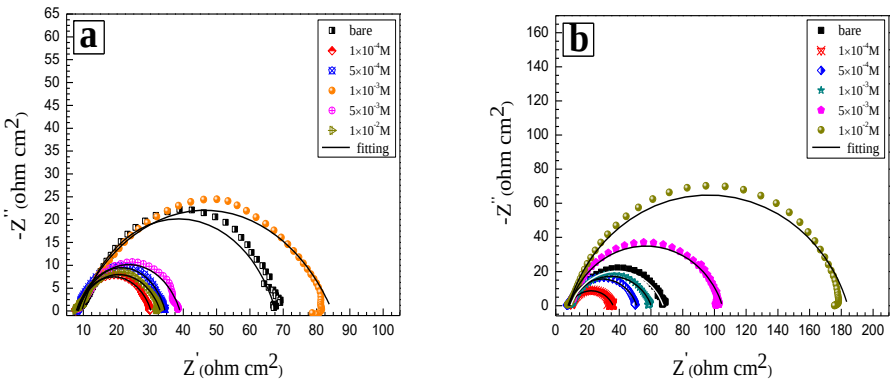

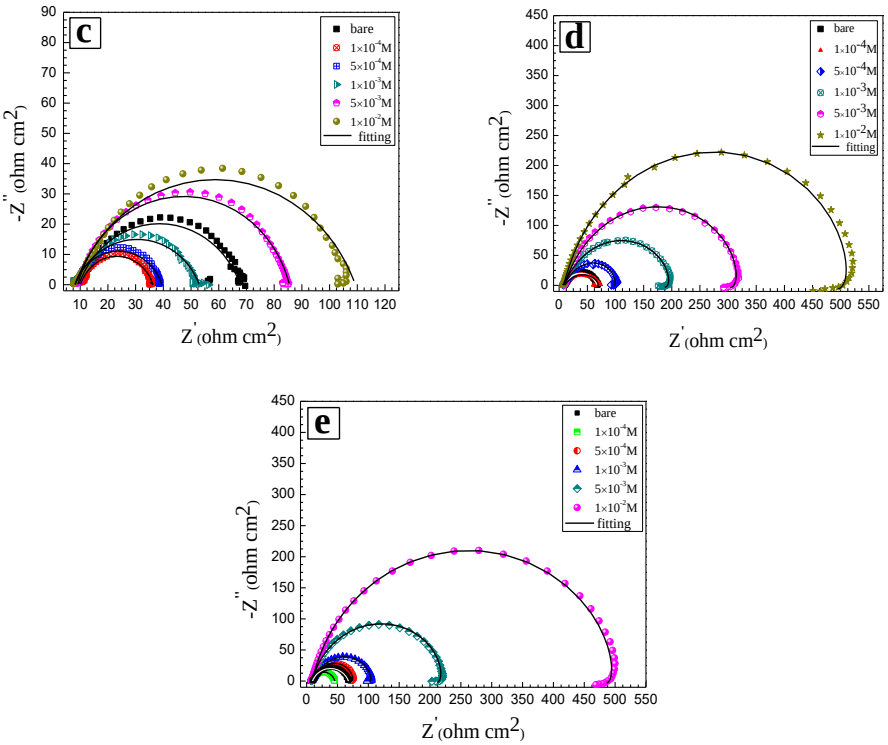

Figure 3. Carbon steel working electrode in the hydrochloric acid solution with PA and BAB or different molar ratio or without corrosion inhibitor test Nyquist complex plan, (a) is PA, (b) is BAB, (c) is PA : BAB = 1:1, (d) is PA : BAB = 1:2, (e) is PA : BAB = 1:3, the solid line is the impedance fitting curve.

The key objective of EIS experiments is to provide insight into the characteristics and kinetics of electrochemical processes occurring on CS without and with different molecular layers of different inhibitor molecules in HCl. The Nyquist plots recorded for CS with different inhibitor molecules in HCl are shown in Figure 3. All the Nyquist plots display one capacitive loop in the solutions with and without inhibitors, which indicates a traditional and simple electrochemical process[23]. The Nyquist plots are not exact semicircles due to the dispersion effect and the instability of the electrode surface.

Figure 4. Electrical equivalent circuit diagram used for modeling WE/solution interface in 0.5 mol·L-1 HCl solution.

All EIS spectra are fitted using the equivalent circuit shown in Figure 4, which is a parallel combination of the charge transfer resistance (*R*ct) and the constant phase element (*CPE*), both in series with the solution resistance (*R*s)[33]. The double layer capacitance (C_{dl}) is replaced by the *CPE*, and the admittance and impedance of the *CPE* can be defined from Eq. (2) and (3):

$$Y_{CPE} = Y_0(j\omega)^n \quad (2)$$

$$Z_{CPE} = \frac{1}{Y_0}(j\omega)^{-n} \quad (3)$$

where Y_0 is the modulus, n is the deviation parameter and ω is the angular frequency. Accordingly, the values of C_{dl} can be calculated using Eq. (4)[34, 35]:

$$C_{dI} = Y_0^{1/n} \; R_{ct}^{(1-n)/(n)} \quad (4)$$

The inhibition efficiencies (η_R) of different inhibitor molecules are estimated with the following Eq. (5):

$$\eta_R = \frac{R_{ct} - R_{ct}^0}{R_{ct}} \times 100\% \quad (5)$$

where R_{ct}^0 and R_{ct} are the charge transfer resistance of CS in HCl without and with inhibitor molecules, respectively.

Table 3 shows the fitted data and the calculated corrosion efficiencies from the impedance plots (Figure 3) of the CS electrode with and without different inhibitor molecules for an immersion time of 1 h. The R_{ct} values represent the charge transfer resistance of CS in HCl. This result indicates the synergistic effect of the PA and BAB molecules is adsorbed on the active sites of the CS surface at a molar ratio of 1:2, and the maximal efficiency is with the concentrations 1×10^{-2} M:2×10^{-2} M. Actually, the existence of inhibitors improves the values of Rct and decreases both the C_{dl} and i_{corr} values, signifying that inhibitors hinder CS corrosion by adsorption among acid/metal[36].

Table 3. Carbon steel working electrode Measured impedance in the hydrochloric acid solution with or without inhibitor.

Assembly molecules	Concentration (mol.L^{-1})	Molar Ratio	Immersion time(h)	Rs (Ω cm^2)	Rct (Ω cm^2)	*CPE* Y_0(μΩ^{-1} S^n cm^2)	*CPE* n	C_{dI} (μF cm^2)	η (%)
Bare	0	--	--	9.55	58.16	82.54	0.77	17.05	--
PA	1×10-4	--	1	7.89	22.43	483.92	0.75	105.76	-159.29
	5×10^{-4}	--	1	8.32	26.23	381.99	0.79	118.51	-121.73
	1×10-3	--	1	8.21	76.48	406.64	0.67	71.13	23.95
	5×10^{-3}	--	1	8.5	30.52	387.86	0.75	86.66	-90.56
	1×10-2	--	1	8.29	24.83	524	0.73	102.5	-134.23
BAB	2×10^{-4}	--	1	9.18	26.55	486.6	0.77	131.01	-119.06
	1×10^{-3}	--	1	7.81	43.15	240.99	0.79	75.39	-34.79
	2×10^{-3}	--	1	9.43	50.71	286.53	0.76	75.07	-14.69
	1×10^{-2}	--	1	9.99	93.26	141.08	0.86	97.77	37.64
	2×10^{-2}	--	1	8.25	175.8	113.69	0.81	45.23	66.92
PA/BAB	1×10-4	1:1	1	10.16	26.11	314.44	0.79	90.11	-122.75
	5×10^{-4}	1:1	1	9.04	30.02	201.88	0.85	80.48	-93.74
	1×10-3	1:1	1	8.17	44.85	250.32	0.75	55.81	-29.68
	5×10^{-3}	1:1	1	9.16	76.34	112.38	0.83	42.76	23.81
	1×10-2	1:1	1	8.52	100.2	111.01	0.8	37.27	41.96
PA/BAB	1×10-4	1:2	1	9.82	61.87	436.5	0.65	59.94	5.99
	5×10^{-4}	1:2	1	10.8	95.37	93.32	0.83	34.26	39.02
	1×10-3	1:2	1	10.23	195.8	56.73	0.82	20.41	70.29
	5×10^{-3}	1:2	1	9.19	314.8	35.92	0.83	14.56	81.52
	1×10-2	1:2	1	7.07	522.2	28.01	0.84	12.86	88.86
PA/BAB	1×10-4	1:3	1	7.87	38.48	270.19	0.78	73.41	-51.14
	5×10^{-4}	1:3	1	8.63	68.59	159.47	0.82	60.91	15.21
	1×10-3	1:3	1	8.21	100.7	147.22	0.76	39.16	42.24
	5×10^{-3}	1:3	1	8.29	214.8	47.16	0.86	22.11	72.92
	1×10-2	1:3	1	7.62	503	28.12	0.85	13.12	88.44

3.3.SEM measurements

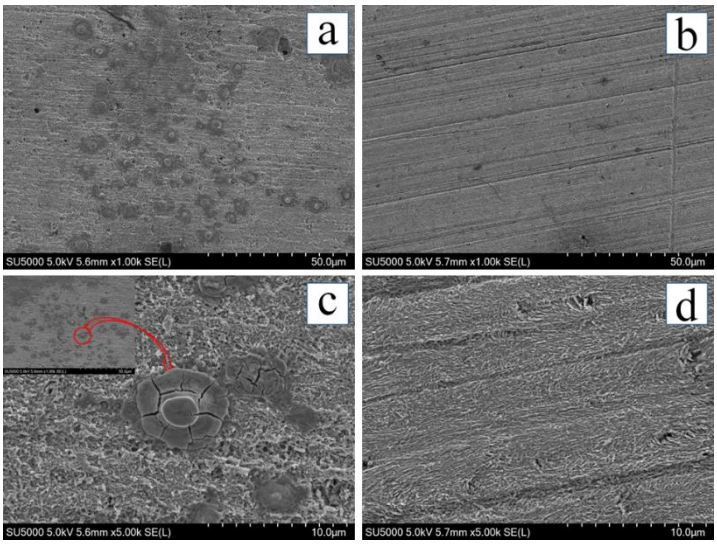

Figure 5. SEM micrograph of corrosion surface of carbon steel after etching for 1 h in 0.5 mol•L^{-1} HCl solution with or without corrosion inhibitor. (a) and (b) are the surface topography and localized topography of the blank steel samples. (c) and (d) are the topography and local magnification of the carbon steel with the addition of corrosion inhibitor.

The microstructures of the CS surfaces immersed in 0.5 M HCl for 0.5 h with and without PA and BAB molecules at a molar ratio of 1:2 with a concentration of 1×10^{-2} M:2×10^{-2} M adsorbed on the metal surface are shown in Figure 5. The CS surface without inhibitor molecule films was corroded in the HCl solution (Figure 5a and Figure 5c). There are some small corrosive holes on the CS surface, which may be caused by the Cl^- ion erosion process. In contrast, the surface of CS covered with the inhibitor molecule films was flat with only some slight scratches on it (Figure 5b and Figure 5d). It is very obvious from the SEM micrographs that the synergy of PA and BAB molecules exerts an inhibitory effect on the corrosion of carbon steel.

3.4. Quantum chemical calculation and dynamic molecular simulation

3.4.1. Quantum chemical calculations

The results of the above experiments provide evidence that PA and BAB molecules and their synergistic effect can protect CS from corrosion in HCl by chemical adsorption on the CS surface. To determine the corrosion mechanism of the inhibitor molecules, quantum chemical calculations were used for further study. The results of the molecular geometric construction and the frontier molecular orbital surfaces optimized by Gaussian are shown in Figure 6. The data from the frontier molecular orbital surfaces calculated by quantum chemical calculations are shown in Table 4. The frontier molecular orbital energies include E_{LUMO} and E_{HOMO}. The energy of E_{HOMO} represents the ability of the molecule to provide electrons. The higher the value of the frontier molecular orbital energy is, the easier it is to provide an electron for the unfilled molecular orbitals of suitable acceptor molecules with low energy. In contrast, the energy of E_{LUMO} represents the ability of a molecule to accept electrons.

The lower the value of the frontier molecular orbital energy is, the more likely it is to accept electrons. With respect to the inhibitor molecules, the low value of E_{LUMO} indicates that the inhibitor molecules more easily accept an electron and accommodate the redundant charge of the metal surface. Thus, the adsorption energy between the inhibitors and iron surface will decrease while the energy gap ($\Delta E = E_{LUMO} - E_{HOMO}$) increases[37, 38].

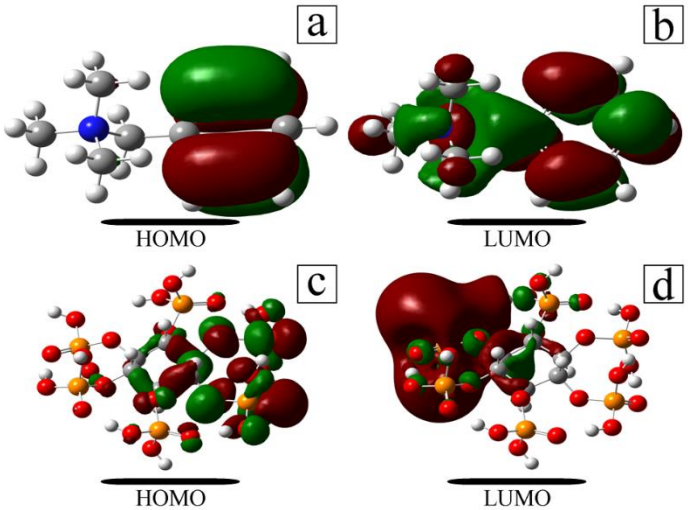

Figure 6. Corrugator molecular frontline orbit distribution, (a) and (b) are BAB molecules, (c) and (d) are phytic acid molecules.

According to Koopmans's theorem, the ionization potential (I) is estimated by $I = -E_{HOMO}$ and the electron affinity (A) is estimated by $A = -E_{LUMO}$[39-41]. The values of χ and γ for the inhibitor molecules were calculated from Eq. (6) and (7)[42] :

$$\chi = \frac{I + A}{2} \quad (6)$$

$$\gamma = \frac{I - A}{2} \quad (7)$$

Therefore, the change in the number (ΔN) of electrons transferred is calculated by Eq. (8)[43, 44]:

$$\Delta N = \frac{\chi_{Fe} - \chi_{inh}}{2(\gamma_{Fe} + \gamma_{inh})} \quad (8)$$

where χ_{Fe} and χ_{inh} are the absolute electronegativity of the iron atom and inhibitor molecules, and γ_{Fe} and γ_{inh} are the global hardness of the iron atom and inhibitor molecules. In this study, the theoretical values of χ_{Fe} and γ_{Fe} are taken as 7 eV and 0 eV[41, 45].

The calculated results are reported in Table 4. The ΔN values represent the inhibitive performance of the inhibitors resulting from electron donation. If $\Delta N < 3.6$, a higher ΔN implies the better electron donation capability and inhibition efficiency of the inhibitor molecules[46]. From Table 4, it is clear that the inhibition efficiency of PA is superior to that of BAB.

Table 4. Quantum chemical parameters of corrosion inhibitor molecules.

Assembly molecule	E_{HOMO} (eV)	E_{LUMO} (eV)	ΔE (eV)	M (Debye)	$\chi=(I+A)/2$	$\gamma=(I-A)/2$	ΔN	η_{max}(%)
BAB	-10.364	-4.215	6.148	5.957	7.290	3.074	-0.047	66.92
PA	-8.171	-1.235	6.936	15.117	4.703	3.468	0.331	23.95

4.2. Dynamic simulation

Table 5. The binding energy of the corrosion inhibitor molecule and the maximum protection efficiency

Assembly molecules	$E_{adsorption}$(eV)	$E_{binding}$(eV)	η_{max}(%)
BAB	-3.0384	3.0384	66.92
PA	-8.2593	8.2593	23.95

Using molecular dynamics simulations, we can obtain the energy of adsorption when the entire system reaches thermal and energetic equilibrium. Then, the energy of the inhibitor molecules adsorbed on the iron surface Fe (1 1 0) can be expressed by means of the binding energy. The adsorption energy and binding energy in the system are calculated by Eq. (6) and (7):

$$E_{adsorption} = E_{total} - (E_{surface+solution} + E_{inhibitor+solution}) + E_{solution} \quad (6)$$

$$E_{binding} = - E_{adsorption} \quad (7)$$

where E_{total} is the total potential energy of the system, $E_{surface+solution}$ and $E_{inhibitor+solution}$ are the potential energies of the system without the inhibitor and the system without the CS surface, respectively, and $E_{solution}$ is the potential energy of all of the water molecules. The calculated binding energies and experimental inhibition efficiencies are shown in Table 5.

As shown in Figure 7, it is clear that the inhibitor molecules can absorb to the iron surface Fe (1 1 0), which is attributed to the frontier molecular orbital being the occupied molecular orbital and the unoccupied molecular orbital. In addition to the chemical bond, there are some other intermolecular forces between the inhibitor molecules and the iron surface. For example, van der Waals interactions, metal complexation and H bonding. The results of the quantum chemical calculations and dynamic molecular simulations show the same conclusion; i.e., the synergistic inhibitors PA and BAB have corrosion inhibition capacities greater than that of PA or BAB, and the results of the electrochemical measurements also support this conclusion.

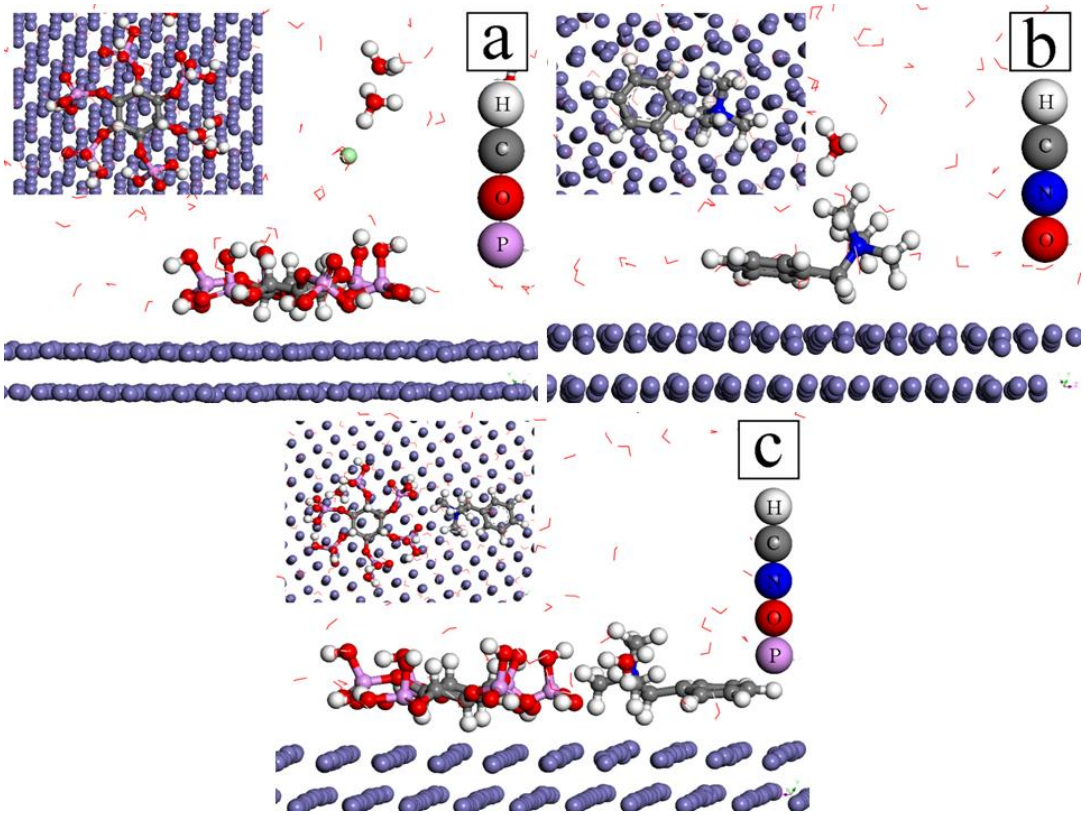

Figure 7. Adsorption equilibrium configuration of corrosion inhibitor molecules on carbon steel in molecular dynamics simulation of hydrochloric acid, (a) is a PA molecule, (b) is a BAB molecule, and (c) is a PA and BAB complex molecule.

4. CONCLUSIONS

A study of the inhibition abilities if environment-friendly synergistic inhibitors PA and BAB on CS surfaces was conducted using EIS polarization measurements. A theoretical study was used to elucidate the inhibition mechanism. From the experiment above, the following points were concluded:

(1) A synergistic inhibitor of PA and BAB can adsorb onto the CS surface and form molecule films that can prevent CS corrosion in 0.5 M HCl. The inhibition efficiency changes with different concentrations and molar ratios.

(2) The synergistic inhibitor of PA and BAB molecule films acts as a mixed-type inhibitor by decreasing both anodic metal dissolution and cathodic hydrogen reduction reactions. Electrochemical measurements show that the synergistic inhibitor PA and BAB molar ratio of 1:2 has the highest inhibition efficiency.

(3) Quantum chemical calculations and dynamic simulations indicate that PA and BAB can absorb on the CS surface by chemisorption. The synergistic inhibitor of PA and BAB absorbs more closely on the iron surface than the PA or BAB molecules alone.

ACKNOWLEDGEMENTS
This work was funded by the Nature Science Foundation of Guangxi Province of China (No. 2016GXNSFAA380061), Guangxi Key Laboratory of Electrochemical and Magnetochemical Functional Materials (EMFM20161104, EMFM20161203).

References

1. J.-J. Park, E.-K. Park, G.-J. Lee, C.-K. Rhee, M.-K. Lee, *Appl. Surf. Sci.,* 415 (2017) 143-148.
2. M. Messali, H. Lgaz, R. Dassanayake, R. Salghi, S. Jodeh, N. Abidi, O. Hamed, *J. Mol. Struct.,* 1145 (2017) 43-54.
3. P.B. Raja, M. Ismail, S. Ghoreishiamiri, J. Mirza, M.C. Ismail, S. Kakooei, A.A. Rahim, *Chem. Eng. Commun.,* 203 (2016) 1145-1156.
4. P. Roy, A. Pal, D. Sukul, *RSC. Adv.,* 4 (2014) 10607.
5. C. Hao, R.-H. Yin, Z.-Y. Wan, Q.-J. Xu, G.-D. Zhou, *Corros. Sci.,* 50 (2008) 3527-3533.
6. Y. Hao, L.A. Sani, T. Ge, Q. Fang, *Appl. Surf. Sci.,* 419 (2017) 826-837.
7. M.A. Chidiebere, E.E. Oguzie, L. Liu, Y. Li, F. Wang, *Ind. Eng. Chem. Res.,* 53 (2014) 7670-7679.
8. C.-c. Li, X.-y. Guo, S. Shen, P. Song, T. Xu, Y. Wen, H.-F. Yang, *Corros. Sci.,* 83 (2014) 147-154.
9. Y. Lei, N. Sheng, A. Hyono, M. Ueda, T. Ohtsuka, *Prog. Org. Coat.,* 77 (2014) 774-784.
10. X. Gao, C. Zhao, H. Lu, F. Gao, H. Ma, *Electrochim. Acta.,* 150 (2014) 188-196.
11. J. Chen, Y. Song, D. Shan, E.-H. Han, *Corros. Sci.,* 74 (2013) 130-138.
12. F. Cao, J. Wei, J. Dong, W. Ke, *Corros. Sci.,* 100 (2015) 365-376.
13. S.A.A. El-Maksoud, *J. Electroanal. Chem.,* 565 (2004) 321-328.
14. M. Lavania, P.M. Sarma, A.K. Mandal, S. Cheema, B. Lai, *J. Environ. Sci-China.,* 23 (2011) 1394-1402.
15. Z. Zhang, N. Tian, X. Li, L. Zhang, L. Wu, Y. Huang, *Appl. Surf. Sci.,* 357 (2015) 845-855.
16. M.J. Frisch, G.W. Trucks, H.B. Schlegel, G.E. Scuseria, M.A. Robb, J.R.Cheeseman, J.A. Montgomery Jr., T. Vreven, K.N. Kudin, J.C. Burant, J.M.Millam, S.S. Iyengar, J. Tomasi, V. Barone, B. Mennucci, M. Cossi, G. Scalmani,N. Rega, G.A. Petersson, H. Nakatsuji, M. Hada, M. Ehara, K. Toyota, R. Fukuda,J. Hasegawa, M. Ishida, T. Nakajima, Y. Honda, O. Kitao, H. Nakai, M. Klene, X.Li, J.E. Knox, H.P. Hratchian, J.B. Cross, C. Adamo, J. Jaramillo, R. Gomperts, R.E.Stratmann, O. Yazyev, A.J. Austin, R. Cammi, C. Pomelli, J.W. Ochterski, P.Y.Ayala, K. Morokuma, G.A. Voth, P. Salvador, J.J. Dannenberg, V.G. Zakrzewski,S. Dapprich, A.D. Daniels, M.C. Strain, O. Farkas, D.K. Malick, A.D. Rabuck, K.Raghavachari, J.B. Foresman, J.V. Ortiz, Q. Cui, A.G. Baboul, S. Clifford, J.Cioslowski, B.B. Stefanov, G. Liu, A. Liashenko, P. Piskorz, I. Komaromi, R.L.Martin, D.J. Fox, T. Keith, M.A. Al-Laham, C.Y. Peng, A. Nanayakkara, M.Challacombe, P.M.W. Gill, B. Johnson, W. Chen, M.W. Wong, C. Gonzalez, J.A.Pople, Gaussion 03, Gaussian Inc, Wallingford, CT, 2004.
17. K.F. Khaled, *Electrochim. Acta.,* 53 (2008) 3484–3492.
18. S. Satoh, H. Fujimoto, H. Kobayashi, *J. Phys. Chem,* 110 (2006) 4846–4852.
19. Z. Zhang, N.C. Tian, L. Zhang, L. Wu, *Corros. Sci.,* 98(2015),438-449
20. Materials Studio, Revision 6.0, Accelrys Inc., *San. Diego.,* USA, 2011.
21. S. Satoh, H. Fujimoto, H. Kobayashi, *J. Phys. Chem.,*110 (2006) 4846–4852.
22. Z. Zhang, N.C. Tian, X.D. Huang, W. Shang, L. Wu, *RSC. Adv.,* 6 (2016) 22250-22268.
23. Junlei Tang, Yuxin Hu, Hu Wang, Yuanqiang Zhu, Yuan Wang1, Zhen Nie, Yingying Wang, Bernard Normand, *Int. J. Electrochem. Sci.,* 14 (2019) 2246 – 2264.
24. M. K. Pavithra, T. V. Venkatesha, M. K. PunithKumar, H. C. Tondan, *Corros. Sci.,* 60 (2012) 104–111.
25. M. Finˇsgar, *Corros. Sci.,* 72 (2013) 82–89.

26. A. ElBribri, M. Tabyaoui, B. Tabyaoui, H. ElAttari, F. Bentiss, *Mater. Chem. Phys.*, 141 (2013) 240–247.
27. M. A. Abu-Dalo, N. A. F. Al-Rawashdeh, A. Ababneh, *Desalination.*, 313 (2013)105–114.
28. Y. Yan, W. Li, L. Cai, B. Hou, *Electrochim. Acta.*, 53 (2008) 5953-5960.
29. A.K. Satapathy, G. Gunasekaran, S.C. Sahoo, K. Amit, P.V. Rodrigues, *Corros. Sci.*, 51 (2009) 2848-2856.
30. Samar .Y. Al-Nami, *Int. J. Electrochem. Sci.*, 14 (2019) 3986-4002.
31. Yanhua Zhu, Liqiang Zhao, Pingli Liu, Peixin Chen, Weidong Tao, Int. *J. Electrochem. Sci.*, 14 (2019) 1331 – 1341.
32. R.K. Gupta, K. Mensah-Darkwa, J. Sankar, D. Kumar, *T. Nonferr. Metal. Soc.*, 23 (2013) 1237-1244.
33. H. Ashassi-Sorkhabi, E. Asghari, *Electrochim. Acta.*, 54 (2008) 162-167.
34. E. McCafferty., *Introduction to Corrosion Science*, Springer, (2010) Dordrecht, Heidelberg, London, NewYork.
35. B. Hirschorn, M.E. Orazem, B. Tribollet, V. Vivier, I. Frateur, M. Musiani, *Electrochim. Acta.*, 55 (2010) 6218-6227.
36. A. S. Fouda, S. A. Abd El-Maksoud, A. El-Hossiany, A. Ibrahim, *Int. J. Electrochem. Sci.*, 14 (2019) 2187 – 2207
37. I.B. Obot, N.O. Obi-Egbedi, *Corros. Sci.*, 52 (2010) 198-204.
38. L. Herrag, B. Hammouti, S. Elkadiri, A. Aouniti, C. Jama, H. Vezin, F. Bentiss, *Corros. Sci.*, 52 (2010) 3042-3051.
39. H. Tian, W. Li, K. Cao, B. Hou, *Corros. Sci.*, 73 (2013) 281-291.
40. M. A. Hegazy, A. M. Badawi, S. S. Abd El Rehim and W. M. Kamel, *Corros. Sci.*, 69 (2013) 110–122.
41. F. Zhang, Y. Tang, Z. Cao, W. Jing, Z. Wu, Y. Chen, *Corros. Sci.*, 61 (2012) 1-9.
42. K. Zhang, B. Xu, W. Yang, X. Yin, Y. Liu, Y. Chen, *Corros. Sci.*, 90 (2015) 284-295.
43. G. Xia, X. Jiang, L. Zhou, Y. Liao, M. duan, H. Wang, Q. Pu, J. Zhou, *Corros. Sci.*, 94 (2015) 224-236.
44. H. Zhao, X. Zhang, L. Ji, H. Hu, Q. Li, *Corros. Sci.*, 83 (2014) 261-271.
45. A. Kokalj, *Chem. Phys.*, 393 (2012) 1-12.
46. H. Ju, Z.-P. Kai, Y. Li, *Corros. Sci.*, 50 (2008) 865-871.

© 2019 The Authors. Published by ESG (www.electrochemsci.org). This article is an open access article distributed under the terms and conditions of the Creative Commons Attribution license (http://creativecommons.org/licenses/by/4.0/).